# A Shell-type Self-assembled Mineralized Adsorbent for Hg(II) Absorption: Synthesis and Performance Studies

**Yang Peng**
Huazhong University of Science and Technology
**Chuxuan Zhang**
Huazhong University of Science and Technology
**Xiaomin Li**
Huazhong University of Science and Technology
**Tianyi Feng**
Huazhong University of Science and Technology
**Xun Gong** ( gx@hust.edu.cn )
Huazhong University of Science and Technology

**Research Article**

**Keywords:** Hg(II) adsorption, Ca-alginate, forming absorbent, shell-type, self-assembly mineralization

**Posted Date:** October 25th, 2021

**DOI:** https://doi.org/10.21203/rs.3.rs-1002264/v1

**Title:**

A shell-type self-assembled mineralized adsorbent for Hg(II) absorption: Synthesis and performance studies

**Author names and affiliations**

Yang Peng, Chuxuan Zhang, Xiaomin Li, Tianyi Feng, Xun Gong*

State Key Laboratory of Coal Combustion, School of Energy and Power Engineering, Huazhong University of Science and Technology, Wuhan 430074, China

***Corresponding author:**

Tel: +86-27-87542417, Fax: +86-27-87545526;

E-mail address: gx@hust.edu.cn

## Graphic abstract

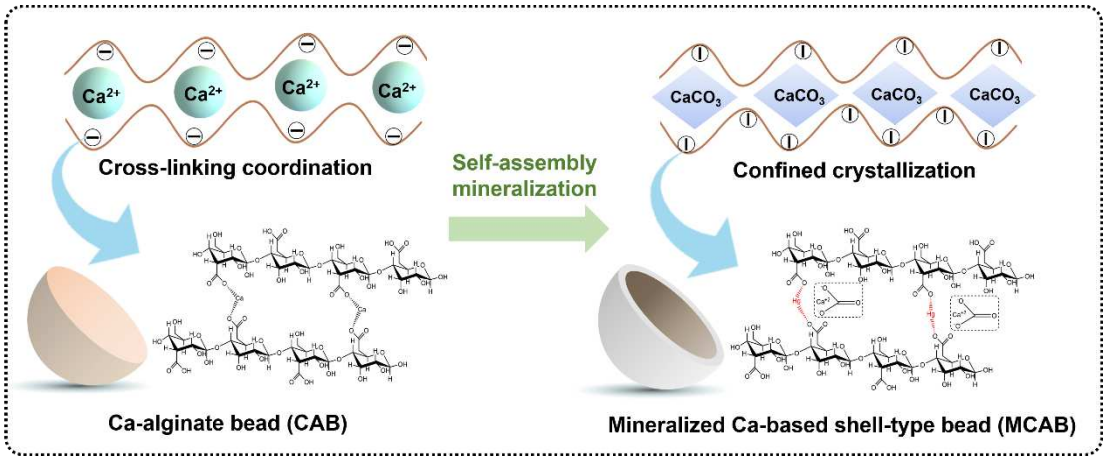

# Highlights

1. A self-assembly mineralization is employed in Ca-based adsorbent modification.

2. The modified Ca-alginate shows a shell-type confined crystallized structure.

3. Remarkably improvement of Hg(II) adsorption is obtained by modification.

4. The ability of anti-wear is enhanced significantly by mineralization.

**Abstract**

For forming adsorbents, the stability of cyclic adsorption is as important as the adsorption properties. In this work, A shell-type self-assembled mineralized adsorbent based on Ca-alginate was synthesized for Hg(II) adsorption. The synthesis process consists of gelation of Ca-based spherical polymer template (CAB) and rate-controlled self-assembly mineralization in bicarbonate solution. A shell-type porous crystal layer is proved to be formed on the surface of the organic polymer template by rate-controlled self-assembly mineralization. The single-factor experiment demonstrates that 1% (MCAB-1) is the optimal concentration of bicarbonate. A maximum adsorption capacity, 48 ± 4 mg/g of MCAB-1 was observed at a pH = 5 in batch test, which was 2.67 times that of the unmodified one, CAB, 18 ± 1 mg/g. Long duration (10 h) adsorption tests showed that MCAB-1 exhibited remarkable performance stability and anti-wear ability (43.2 % removal efficiency and 74.3 % mass retention, compared to 2.7 % and 38.6 % of CAB at pH = 3, respectively). The results show that the adsorption and wear resistance of the modified materials are improved obviously.

**Keywords:** Hg(II) adsorption; Ca-alginate; forming absorbent; shell-type; self-assembly mineralization

## 1. Introduction

Nowadays, human health is seriously menaced by heavy metal emissions[1–5]. Mercury contamination of wastewater especially from coal combustion[6,7], and gold mining, including divalent mercury (Hg(II)) and methyl mercury (Me-Hg), is an

extreme threat to human health because of bioaccumulation in the food chain[8–10]. Therefore, the treatments for mercury-contaminated wastewater have attracted wide attention in recent decades[11,12]. The maximum contaminant level (MCL) for mercury in potable water proposed by the World Health Organization (WHO) and U.S. Environmental Protection Agency (EPA) is set under 0.001 mg/L[13]. Several physical and chemical methods, such as precipitation, coagulation, ion exchange, electrochemical methods, adsorption, membrane processes, and ultra-filtration, have been developed to overcome this problem[11,13,14]. Among them, adsorption is the most widely used because of remarkably high efficiency, easy access & operation, and relatively low cost. The development of adsorbents with high efficiency and environmental protection for specific pollutants is still one of the dominant directions of wastewater treatment technology[11,13,15].

Traditional adsorbents are mainly powder particles. For example, the dominated commercial adsorbents used for heavy metals treatment in sewage are activated carbon powders and their derived products nowadays. Hadi et al. reviewed the research status of aqueous mercury adsorption by activated carbons[16]. Serval aspects including preparation of activated carbon, effect of treatment techniques on mercury removal (physical and chemical activation, sulfurization), effect of adsorption parameters (equilibrium contact time, initial concentration, pH value, temperature, adsorption dosage, and particle size), functional groups, and equilibrium adsorption isotherms were exhaustively reviewed. Moreover, activated carbon derived from various biomass

is reported, such as rice hulls[17], coconut shell[18], apricot stone[19], apple peels[20], pecan shell[21], and so on. In addition to activated carbon, various biomass or microorganisms are also potential feedstock of heavy metal adsorbents, including chitosan[22–27], bacteria[28–35], fungus[36,37], algae[38–42], and so on.

The adsorption materials with excellent properties can be obtained by selecting different raw materials and corresponding modification methods. However, there are some fatal problems in the large-scale commercial utilization of powder adsorbents. Firstly, in the application process of powder adsorbent, rapid and efficient separation is often required, which inevitably leads to the improvement of energy consumption and operation cost. Meanwhile, the recovery efficiency of the adsorbent is relatively low. Given this, the immobilization of adsorbents is quite essential for heavy metals treatment in sewage[43–45]. One of the most widely employed materials is Ca-alginate, which is an ideal forming matrix by the classical “egg-box” model[46]. However, the adsorption capacity of calcium alginate itself is extremely low. To obtain the satisfied adsorption capacity, it is necessary to load additional functional materials with excellent adsorption performance, which will inevitably lead to a significant increase in the preparation cost of the adsorbent. It is a challenge that slashing the costs while retaining the forming and adsorption properties.

At the same time, calcium alginate is a cross-linked organic polymer formed by the chelation of calcium ions. The structure and stability of the materials are seriously affected by the decomposition of the long-chain polymer group under strong acid

conditions because metal ions are easily replaced by hydrogen ions. The damage of this structure will seriously reduce the stability and repeatability of adsorbent in industrial utilization. Therefore, it is necessary to evaluate the long-duration adsorption stability of the forming adsorbent in the solid-liquid environment.

Given this situation, a self-assembly mineralization method to modify the calcium alginate beads is proposed in this work, aiming to remarkably improve the adsorption capacity while maintaining the structural stability of the material. The characterization of the modified beads was conducted by BET, XRD, FTIR, and stereoscopic microscope analysis. The performance of the Hg(II) adsorption process was assessed by the Hg(II) isotherms and kinetic adsorption analysis. Furthermore, the material structural stability was assessed by long-duration adsorption tests.

## 2. Experiment & methods

### *2.1 Chemicals and material preparation*

2 g sodium alginate (Aladdin Ltd., AR, China) powder was dissolved in 100 mL of deionized water followed by being stirred for 40 min at 85 °C. After that, the sodium alginate sol was dropped into 2% wt. $CaCl_2$ (Aladdin Ltd., AR, China) solution by a syringe pump to form a kind of spherical Ca-based polymer, Ca-alginate beads (raw sample, named as CAB). These hydrogel beads were then impregnated and mineralized by 100 mL of $NH_4HCO_3$ solutions (Aladdin Ltd., AR, China) with certain concentrations (0.5%, 1%, and 1.5% wt., which were named as MCAB-0.5, MCAB-1, and MCAB-1.5, respectively) in the stable temperature oscillation shaker at 150 rpm

for certain hours. After that, these samples were washed subsequently until $Ca^{2+}$ and $Cl^-$ ions are undetected in the leachates, followed by drying in a freezer dryer for tests (80 Pa, -50 °C).

*2.2 Morphological characterization*

A high-megapixel camera (D5200, Nikon, Japan) was adopted to observe the changes in the surface morphology before and after modification. The sectional views and micro-topography were obtained separately by a stereomicroscope (Stemi 508, Carl Zeiss, Germany). The surface area and pore size distribution were tested by the BET method, which was conducted at 77 K in an $N_2$ atmosphere by an ASAP 2460 instrument (Micromeritics, USA) after drying at 120 °C for 12 hours. In addition, a VERTEX 70 FTIR system (Bruker, German) with the ATR method was used to investigate the changes in functional groups during adsorption. X-ray diffraction (XRD, Cu Kα radiation, Empyrean, PANalytical B.V.), was employed to observe the composition in the surface morphology of the adsorbents, with 2θ ranging from 10° to 80°.

*2.3 The verification of adsorbent uniformity*

Given that the larger particle sizes of raw and modified samples than that of commercial adsorbent powders in this work, the average mass of the materials should be measured to ensure the uniformity of the materials selected in the subsequent parallel experiments. A random sampling method was adopted for uniformity measurement: 10 groups, 5 spherical particles in each group, were selected randomly from each sample.

The single bead mass $m_{ij}$ of each group of samples was measured ($i$ was the serial number of the sampling group, $j$ was the serial number of single bead in each group, $1 \leq i \leq 10$, $1 \leq j \leq 5$). The average mass $M_i$ and error level $e_i$ of each group of samples can be obtained as:

$$M_i = \frac{\sum_{j=1}^{5} m_{ij}}{5} \quad (1)$$

$$e_i = \frac{\sum_{j=1}^{5} (m_{ij} - M_i)}{5} \quad (2)$$

*2.4 Batch adsorption testing*

A standard solution of Hg(II) (1000 mg/L, GR, Aladdin Ltd.) was used as the metal stock solution. Daily dilutions were carried out to obtain the desired concentration. Although it was proven that the temperature of the aqueous system affected the binding ability of heavy metals for some adsorbents[47–49], the pH value, metal ion concentration, and adsorbent dosage were still the dominant influencing factors for the adsorption process[50]. The temperature in this study was fixed at 30 °C, which was consistent with the actual industrial operation[51].

Batch adsorption testing was conducted in conical flasks, which contained approximately 10 mg of adsorbent and a corresponding volume of Hg(II) ion solution for various solid-to-liquid ratios (0.1, 0.3, 0.5 1, 3, 5, 10 g/L) and stirring at 150 rpm. The effect of different pH values on the adsorption was evaluated by controlling the initial pH values to be 3.07, 4.07, 5.01, and 6.06, which was achieved by mixing 0.1

147 mol/L $HNO_3$ and NaOH solutions. The study of the adsorption isotherms was carried
148 out with a variety of initial ion concentrations (1, 2, 5, 10, 15, 20, 25 mg/L) under the
149 optimal conditions. For the adsorption kinetics study, two groups with 1 mL Hg(II)
150 solution were prepared for kinetics testing. Sampling was arranged at 2, 5, 10, 30, 60,
151 120, and 180 min, respectively. The initial pH and dosage were fixed at the optimal
152 conditions according to the tests above. The mixed solutions after adsorption were
153 centrifuged and filtered by a 0.45 microporous membrane filter and then tested by an
154 inductively coupled plasma optical emission spectrometry (ICP-OES) system
155 (SPECTRO ARCOS, German). Each case was tested 3 times to ensure accuracy.
156 The equilibrium adsorption capacity of the adsorbent was calculated by the
157 following formula[52]:
158 $$q_e = \frac{(C_0 - C_e) \cdot V}{m} \quad (3)$$
159 where $q_e$ was the equilibrium adsorption capacity in mg/g, $C_0$ and $C_e$ were the
160 initial and equilibrium Hg(II) solution concentrations in mg/L, respectively, $V$ was
161 the volume of Hg(II) solution in L and $m$ was the mass weight of adsorbent in g.
162 To evaluate the Hg(II) removal efficiency of adsorbent, another formula was applied
163 as follows:
164 $$\eta = \frac{(C_0 - C_t)}{C_0} \times 100\% \quad (4)$$
165 where $\eta$ was the removal efficiency of adsorbent in % at time t, $C_t$ was the
166 concentration of Hg(II) in mg/L at time t, and $C_0$ was the same parameter as
167 mentioned in equation (3).

*2.5 Adsorption stability evaluation of adsorbents*

Long duration (10 h) adsorption tests were conducted in one 500 mL conical flask containing 300 adsorbent beads and a certain volume of 1 mg/L Hg(II) ions solution (optimal solid-liquid ratio maintained) at 30 °C with various pH values, to simulate the harsh corrosion conditions. After each hour, 3 mL solution and 3 adsorbent beads were sampled for analysis until the test finished. Two parameters, the variation of adsorption capacity and mass weight, were employed to assess the stability of MCAB for Hg(II) adsorption in the liquid system.

## 3. Results and discussion

*3.1 Sample characterization*

The sectional views of four samples were observed by the stereomicroscope, as shown in **Fig. 1**. The images show that the unmodified bead shows a loose network structure. This is due to the crosslinking reaction between calcium ions and alginate polymers. However, this structure could be easily decomposed by ion exchange, ligands exchange, or hydrogen-bond interactions in an aqueous phase[53]. In comparison, a dense homogeneous shell is formed on the surface of the modified pellet. Combined with XRD spectra shown in **Fig. S1**, there is a mineralized calcium carbonate layer on the surface of the shell-type calcium alginate sphere. This is due to the confined crystallization between calcium and carbonate ions from the bicarbonate secondary ionization[54]. As for bicarbonate, the secondary ionization constant is much fainter than the first secondary ionization constant, this determined that the surface

mineralization process of calcium alginate would be milder due to the relatively slow release of carbonate[55]. The concentration of bicarbonate solution was determined to be a significant factor in the formation of the mineralized shell. From the cross-section of modified samples in **Fig. 1**, lower concentration (0.5 % wt.) could lead to forming an irregular mineralized layer, while higher concentration (1.5 % wt.) could result in reuniting and oversaturated crystallization[56].

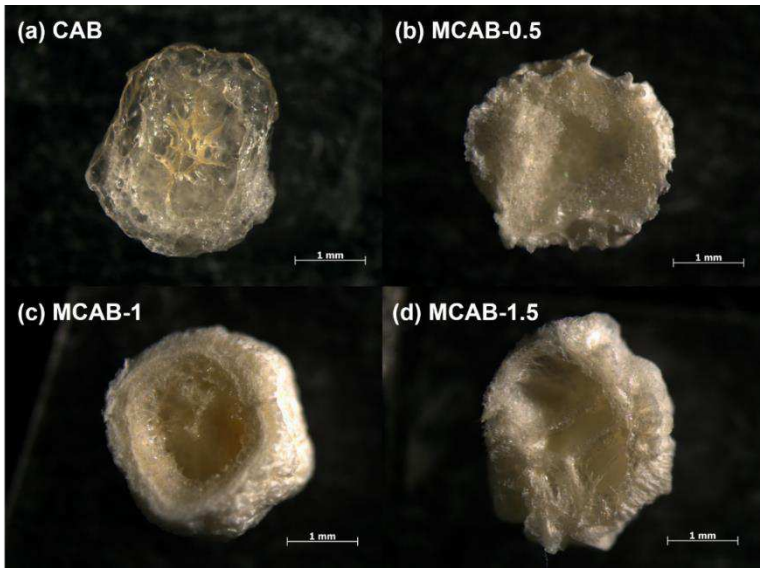


**Fig. 1** Sectional views of CAB and the three MCAB samples

**Table 1** exhibits the porous characteristics of CAB, MCAB-0.5, MCAB-1, and MCAB-1.5 by BET analysis. The specific surface area of MCAB-1, 15.319 $m^2/g$, is proven to be the highest among these four samples compared with those of CAB, 8.201 $m^2/g$; MCAB-0.5, 12.972 $m^2/g$; and MCAB-1.5, 14.772 $m^2/g$, respectively. However, both the pore volume and average pore size of CAB are slightly larger than that of the modified samples, which might be due to the blocking of the network structure on Ca-alginate polymers by the formation and growth of crystal layers[57]. In this work, 1 % of $NH_4HCO_3$ was proven to be the optimal concentration for mineralization.

| Sample | BET surface area ($m^2/g$) | Pore volume ($cm^3/g$) | Average pore width (nm) |
|---|---|---|---|
| CAB | 8.201 | 0.013 | 6.361 |
| MCAB-0.5 | 12.972 | 0.009 | 5.992 |
| MCAB-1 | 15.319 | 0.007 | 5.672 |
| MCAB-1.5 | 14.772 | 0.006 | 5.773 |

205 **Table 1** BET analysis for CAB, MCAB-0.5, MCAB-1, and MCAB-1.5

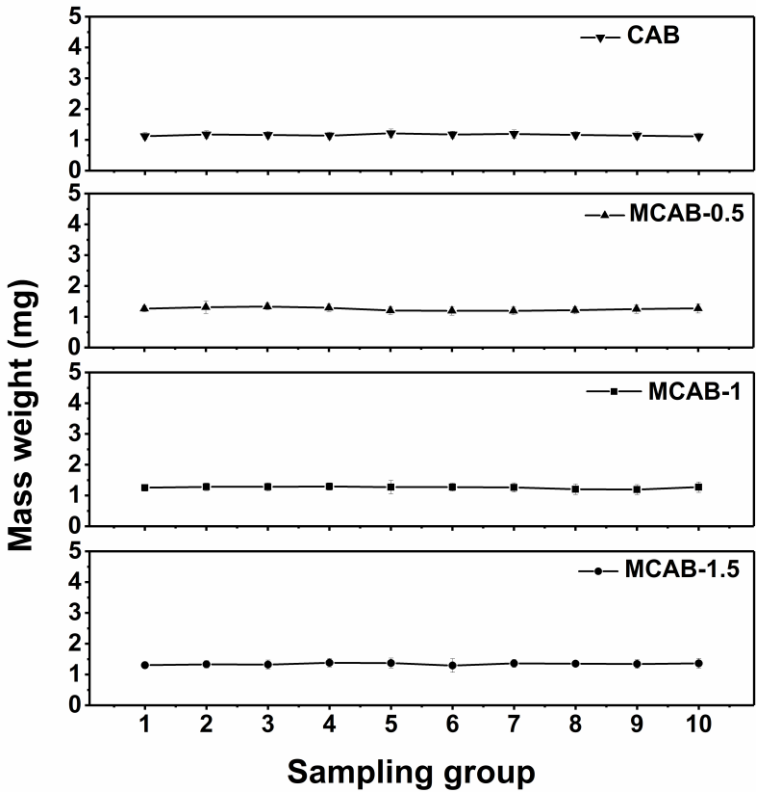


206

207 **Fig. 2** Statistical analysis of the average mass of the single adsorbent particle

208 The statistically mean mass weight of four samples is shown in **Fig. 2**. The average
209 mass weight of single CAB, MCAB-0.5, MCAB-1 and MCAB-1.5 bead is 1.157 ±
210 0.038 mg, 1.250 ± 0.043 mg, 1.256 ± 0.048 mg and 1.340 ± 0.073 mg, respectively.
211 The mass weight of a single modified bead increases with the increase of the

impregnation concentration of $NH_4HCO_3$. Moreover, the mass of each sample is statistically constant within approximately 5% error, which implies that the total sampling quality is in liner with the number of sampling beads. The quality difference between the adsorbent pellets in the same sample is negligible.

### *3.2 Effect of single-factor on the Hg(II) adsorption efficiency*

#### *3.2.1 Effect of dosage*

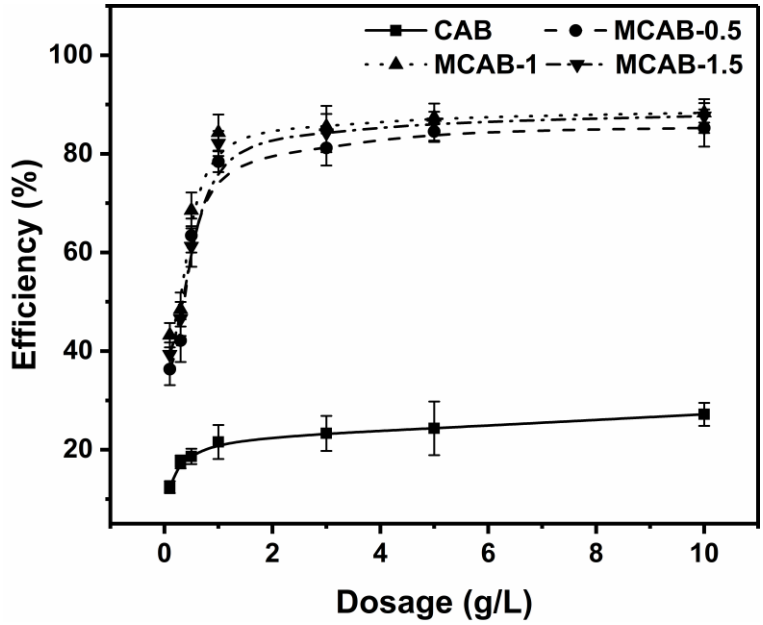


**Fig. 3** Effect of the dosage on the Hg(II) adsorption efficiency (initial Hg(II) concentration = 1 mg/L, oscillation time = 180 min, pH = 5, temperature = 30 °C)

It is widely reported that the dosage of adsorbent has significant impacts on the capability as well as the economical efficiency of metal adsorption. Given that the dispersibility of large particle forming adsorbent is not as good as that of powder materials, it is necessary to adjust the solid-liquid ratio to meet the requirement of higher adsorption efficiency[8,58,59]. **Fig. 3** gives the effect of dosage on the Hg(II) adsorption efficiency of CAB and the three MCAB samples. With the increase of

227 dosage from 0.1 g/L to 1 g/L, the efficiency of each sample increased remarkably.
228 Among them, the efficiency of MCAB-0.5, MCAB-1, and MCAB-1.5 increased from
229 36.3.4 ± 3.2 %, 43.2 ± 2.5 %, and 39.3 ± 2.4 % to 78.4 ±2.1 %, 84.3 ± 3.7 %, and 82.2
230 ± 2.5 %, respectively, compare to that of CAB, from 12.4 ± 1.2 % to 21.6 ± 3.5 %. This
231 indicates that the modified samples can provide more adsorption sites under the same
232 dosage. Further increased the dosage from 1 g/L, the tendency of efficiency
233 improvements slowed down significantly, which implied that the adsorption sites tend
234 to be saturated and the adsorption system gradually reaches dynamic
235 equilibrium[49,60].

236 *3.2.2 Effect of pH*

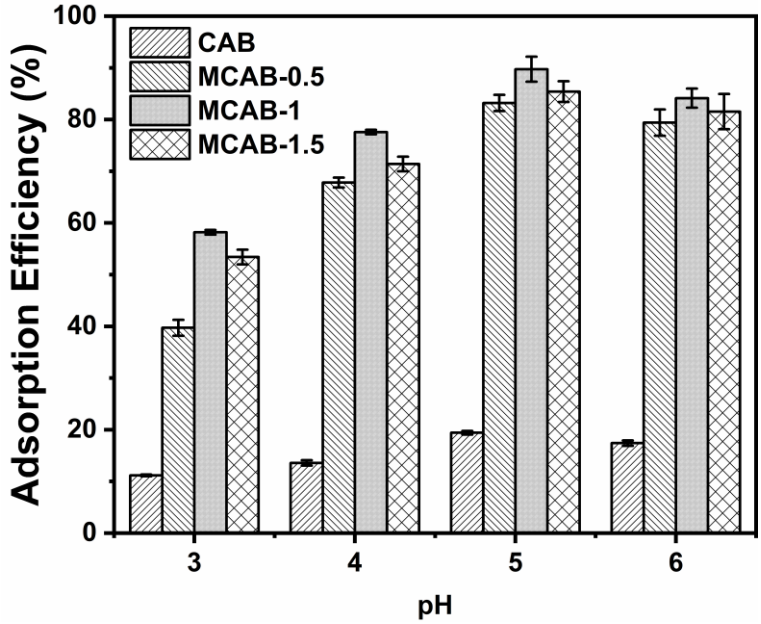


237

238 **Fig. 4** Effect of pH on the Hg(II) adsorption efficiency (initial Hg(II) concentration =
239 1 mg/L, oscillation time = 180 min, dosage = 1 g/L, temperature = 30 °C)

240 pH (especially acidic pH condition) is a very important influence variable in the
241 adsorption process because it not only affects the adsorption efficiency but also has a

great influence on the stability of the material. As shown in **Fig. 4**, the adsorption efficiency increased from pH = 3 to pH = 5 followed by slightly decline from pH = 5 to pH =6. To be specific, the efficiency of MCAB-0.5, MCAB-1, and MCAB-1.5 increased from 38.9 ± 2.3 %, 58.1 ± 0.9 %, and 53.2 ±1.2 % at pH = 3 to 84.2 ± 3.1 %, 89.7 ± 3.3 %, and 83.3 ± 2.3 % at pH = 5, and then decreased to 81.7 ± 4.2 %, 84.1 ± 3.2 %, and 82.1 ± 3.1 % at pH = 6, respectively. Comparing the modified samples, the efficiency of CAB increased from 11.2 ± 0.7 % at pH = 3 to 19.2 ± 0.7 % at pH = 5, then decreased to 17.1 ± 0.8 % at pH = 6. This trend is mainly due to the competitive adsorption of $H^+$, $H_3O^+$, and heavy metal ions under different pH conditions. Under low pH conditions, $H^+$ and $H_3O^+$ occupy the adsorption sites on the adsorbent surface, resulting in the inhibition of Hg(II) during the adsorption process. With the increase of pH, the competitive effect is gradually weakened due to the decrease of $H^+$ and the increase of $OH^-$ in the system. However, under the condition of relatively high pH, Hg(II) is partially converted into neutral or electronegative hydroxides due to hydrolysis, which is also unfavorable for the binding of electronegative functional groups such as hydroxyl and carboxyl groups on the adsorbent surface[61].

According to the single-factor variable control experiment, it can be seen that under the same conditions, both the adsorption ability and environmental tolerance of the mineralized modified samples are significantly better than the original samples. To maximize performance, the combination of 1 g/L, pH = 5 is demonstrated as the optimal operation condition.

### *3.3 The assessment of adsorbent performance in batch adsorption*

#### *3.3.1 Kinetics analysis*

Pseudo first and second order[62] models were used to describe the kinetic process. The pseudo-first-order model[63] can be expressed as follows:

$$q_t = q_e(1-e^{-k_1 t}) . \quad (5)$$

where *t* in min is the contact time between the solid and aqueous phase, $q_e$ in mg/g is the adsorption capacity of the adsorbent at equilibrium, $q_t$ in mg/g is the adsorption capacity of the adsorbent at time *t*, and $k_1$ in $min^{-1}$ is the pseudo-first-order rate constant.

The pseudo-second-order model[62] can be presented as:

$$q_t = q_e \frac{q_e k_2 t}{1+q_e k_2 t} \quad (6)$$

where $q_e$, $q_t$ and $t$ are the same parameters as in equation (5) and $k_2$ in g/mg·min is the pseudo-second-order rate constant.

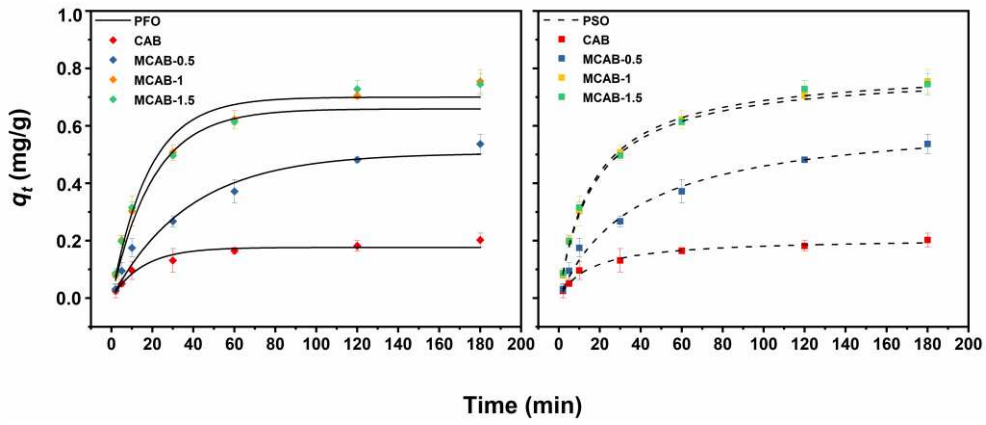


**Fig. 5** Adsorption kinetics models (pH = 5, initial Hg(II) concentration = 1 mg/L, adsorbent dosage = 1 g/L, temperature = 30 °C)

The experimental data fitting with two kinetic models was shown in **Fig. 5** The

280 relevant parameters were calculated (shown in Table S1) using Eqs. (5) and (6). The
281 correlation coefficients ($r^2$) indicate that both models are well fitted to the experimental
282 data. Nonetheless, comparing with pseudo-second-order model ($R^2$= 0.994 ± 0.002,
283 0.991 ± 0.004, 0.993 ± 0.001, and 0.998 ± 0.006), the pseudo-first-order model ($R^2$=
284 0.994 ± 0.002, 0.991 ± 0.004, 0.993 ± 0.001, and 0.998 ± 0.006 for CAB, MCAB-0.5,
285 MCAB-1, and MCAB-1.5, respectively) slightly underestimates the metal uptake of
286 Hg(II) by both adsorbents and is inaccurate to characterize the kinetic mechanism.
287 Furtherly, the equilibrium capacity are 0.18 ± 0.01、0.57 ± 0.01、0.79 ± 0.01, and 0.78
288 ± 0.02 for CAB, MCAB-0.5, MCAB-1, and MCAB-1.5, respectively, calculated by the
289 pseudo-second-order fitting model. This indicates that the intrinsic adsorption capacity
290 was improved obviously by self-assembly mineralization. Based on the comparison of
291 adsorption rate constants of the pseudo-second-order model, i.e. $k_2$ (MCAB-0.5) < $k_2$
292 (MCAB-1.5) ~ $k_2$ (MCAB-1) << $k_2$ (CAB), implying that the adsorption rate was
293 significantly improved by modification. As for the relatively higher $k_2$ of MCAB-0.5
294 compared to the other two modified samples, this probably is due to the lower
295 adsorption capacity requiring a shorter time to reach equilibrium.

296 *3.3.2 Adsorption isotherms*

297 Langmuir and Freundlich's modes were applied to calculate the isotherm parameters.
298 The Langmuir isotherm is described by the following equation[52]:

299
$$q_e = \frac{q_m k_L C_e}{1 + k_L C_e} \tag{7}$$

300 where $q_e$ is the equilibrium capacity of the adsorbent in mg/g, $C_e$ is the

concentration of Hg(II) ions in the liquid at equilibrium in mg/L, and $q_m$ in mg/g is the maximum adsorption capacity of the adsorbent by calculation. $k_L$, the so-called Langmuir isotherm adsorption constant in L/mg, refers to the bonding energy of sorption.

The Freundlich isotherm model[52] is expressed by the following equation:

$$q_e = K_F C_e^{1/n} \tag{8}$$

where $K_F$ in (mg/g)(1/mg)$^{1/n}$ is the Freundlich constant and $q_e$, $C_e$ are the same variables as in equation (7).

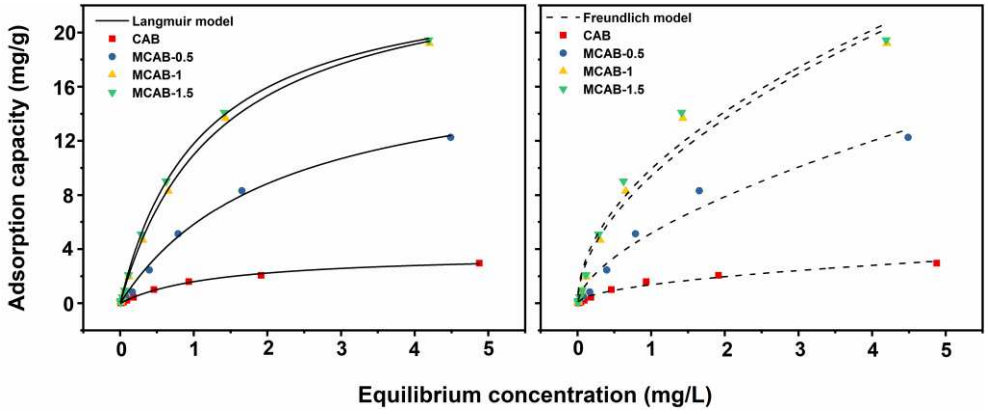


**Fig. 6** Adsorption isotherm fitting curves (pH = 5, oscillation time = 180 min. adsorbent dosage = 1 g/L, test temperature = 30 °C)

The surface properties and affinities of the adsorbent can be expressed by certain constants that characterize the adsorption isotherms, presented in **Fig. 6**. The Langmuir adsorption isotherm constants ($q_m$ and $K_L$), Freundlich isotherm constants ($K_F$), and correlation coefficients ($R^2$) for the adsorption of Hg(II) on the adsorbents are presented in **Table S2**. The maximum capacity $q_m$ determined from the Langmuir isotherm indicates the limiting capacity of the absorbent for Hg(II) ions. It was found that the

maximum capacity $q_m$ for the MCAB-1 sample of 48 ± 1 mg/g was much higher than that for CAB of 18 ± 1 mg/g. The correlation coefficients ($R^2$) for MCABs and CABs show that the Langmuir isotherm model is properly used to describe both adsorbents, which indicates that mono-layer adsorption of heavy metal ions is formed on the outer surface of adsorbents[47].

The Freundlich model is used to characterize the adsorption on a heterogeneous surface and is not limited to mono-shell formation. However, the values of the correlation coefficients ($R^2$) calculated by the Freundlich isotherm model (0.970 ± 0.006, 0.968 ± 0.003, 0.965 ± 0.003, and 0.960 ± 0.009) are lower than those from Langmuir model (0.996 ± 0.002, 0.995 ± 0.004 , 0.998 ± 0.003, and 0.999 ± 0.006 for CAB, MCAB-0.5, MCAB-1, and MCAB-1.5, respectively), which indicates that the Freundlich model is unacceptable for describing the adsorption process.

On account of the comparison of adsorption kinetics and isothermal adsorption model fitting, it can be obtained that self-assembly mineralization modification can conspicuously improve the adsorption rate of materials as well as the binding efficiency of adsorption sites, and significantly promotes the improvement of the adsorption capacity of materials.

*3.4 The evolution of functional groups during batch adsorption*

FTIR measurements on MCABs and CABs before and after Hg(II) adsorption were investigated as well (shown in **Fig. S3**). The bands at 3266 $cm^{-1}$ in the sample (a) were attributed to the hydroxyl stretching vibration mode. The same results were reflected

for (b) at 3193 $cm^{-1}$, (c) at 3206 $cm^{-1}$, and (d) at 3185 $cm^{-1}$, which were observed to move to lower frequencies because of the hydrogen-bond interaction during the impregnation and adsorption. The weak bands observed at 2925 and 2852 $cm^{-1}$ for sample (a) were due to the symmetric and asymmetric stretching bands of -$CH_2$, which moved to 2988 and 2910 $cm^{-1}$ along with 2995 and 2921 $cm^{-1}$ for samples (b) and (d), respectively. The bands at 1598 and 1415 $cm^{-1}$ for sample (a) were attributed to the symmetric and asymmetric stretching bands of -$COO^-$ groups, which shifted to 1590 and 1410 $cm^{-1}$ for both (b) and (d), while they disappeared for sample (c). The wide peak at 1414 $cm^{-1}$ for sample (c) was found to be the asymmetric variable angle vibration of $NH_4^+$ ions due to the $NH_4HCO_3$ coating. The C-O-C stretching vibration peak was observed at 1028 $cm^{-1}$ for all four of these samples and declared that the condensation between monomer G and M blocks cannot be interrupted by either $NH_4HCO_3$ modification or Hg(II) adsorption. Additionally, it is found that the outer bending vibration peak of $CaCO_3$ was observed at 882 $cm^{-1}$ for sample (c), which indicated that $Ca^{2+}$ ions trapped by -$COO^-$ in polymers before modification might be grabbed by hydrolyzed $CO_3^{2-}$ ions from $NH_4HCO_3$ to further form the $CaCO_3$ microcrystalline structure[64], which is consistent with the study mentioned above.

### *3.5 Effect of mineralization on the stability of the adsorption efficiency and material structure*

Long-duration (10 h) adsorption was conducted to investigate the effect of mineralization on the stability of the adsorption efficiency and retardation of material

wear. Fig. 7 shows the changes of mass weight and adsorption efficiency during long-duration adsorption at pH =3. Both two indices of all samples decreased as the adsorption progress. Specifically, after 10 h adsorption, the mass weight of CAB, MCAB-0.5, MCAB-1, and MCAB-1.5 were 38.6 %, 61.2%, 74.3% and 74.3% of each initial mass, respectively. Meanwhile, the efficiency of these four sample decreased from 10.1 %, 38.2 %, 57.4 %, and 56.4 % to 2.7 %, 21.4 %, 43.2 %, and 39.7 %, respectively. In addition, the dynamic changes of quality and efficiency indicate that there is a positive correlation between them. This improvement indicated that mineralization not only improved the adsorption efficiency but also enhanced the stability of adsorbent performance.

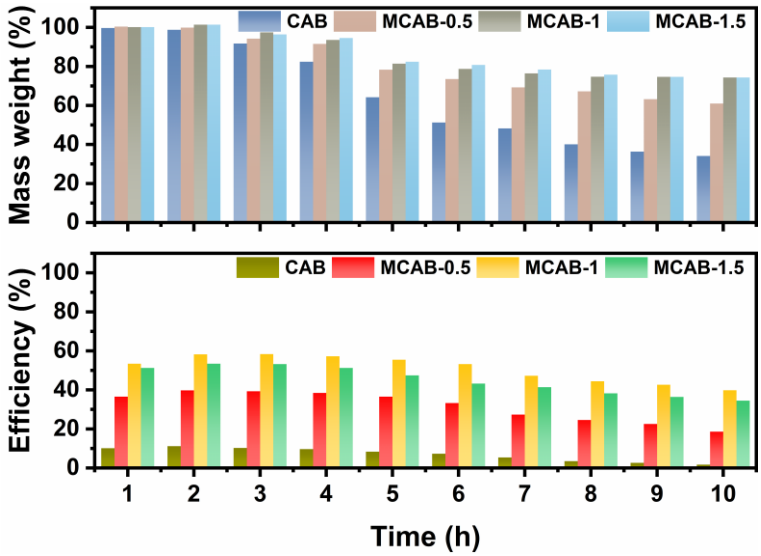


**Fig. 7** Mass weight and adsorption efficiency during adsorption process (pH = 3, initial Hg(II) concentration = 1 mg/L, dosage = 1 g/L, temperature = 30 °C)

In another assessment result, macroscopic morphological changes for CAB and MCABs are represented in **Fig. S2**. For CAB, the raw bead is a ball with good sphericity. After 10 h of adsorption, different degrees of disintegration are observed in various pH

conditions. At a pH = 3, the bead is collapsed, which is in accordance with the weight ratio tests. After mineralization, the surfaces of raw modified beads, MCAB-0.5, MCAB-1, and MCAB-1.5, are whiter and more substantial compared with CAB. Additionally, the completeness of the materials is much better than that of CAB. The concentration of $NH_4HCO_3$ shows a dominant effect on morphological changes. This is mainly because various carbonate concentration leads to different calcium carbonate crystallization rate in the growth process of microcrystalline so that the structure bears a different degree of local stress in the confined crystallization process. As the mineralization unit grows, the stress changes the local structure more obviously, and finally leads to different macroscopic mineralization layers[64].

### *3.6 Mechanism of mercury adsorption by self-assembly mineralized shell-type adsorbent*

The initial structure of calcium alginate beads is a macromolecular reticular polymer that is cross-linked by calcium ions. With the impregnation of $NH_4HCO_3$, the calcium ions and carbonate ions produced by ammonium bicarbonate secondary hydrolysis were gradually combined and crystallized by self-assembly mineralization. Due to the existence and hindrance of the uronic acid polymer chain, the mineralized crystallization is gradually transformed to the confined crystallization, leading to the formation of a large number of amorphous calcium carbonate mineralized layers. Moreover, with the calcium ions in the outer layer of the microsphere mineralized firstly, the difference between internal and external concentration will lead to diffusional

pressure difference. This difference results in the transfer of inner ions to the external, depositing to mineralization and forming a shell-type spherical structure. To some extent, the formation of a mineralized layer promotes the transformation of structure from dense polymer crosslinking to the organic-inorganic doped skeleton with a large specific surface area and high porosity. On the other hand, a large number of chelated carboxylic acids on the polymer chain are released and activated because of the trapping of calcium ions by carbonates, which also provides abundant binding sites for mercury ions.

## 4. Conclusions

In the process of sewage treatment by adsorption, there are mounts of drawbacks such as high energy consumption in solid-liquid separation, serious wear of materials, and recovery of adsorbent particles. Given this, it is imperative to develop a high-performance anti-wear forming adsorbent. In this work, a kind of self-assembly mineralized shell-type adsorbent was synthesized and employed to adsorb Hg(II) in the aqueous phase. It is found that the optimal sample set, MCAB-1, shows a significant enhancement for Hg(II) adsorption with maximum adsorption of 48 ± 1 mg/g in 3 h at pH = 5, which is 2.67 times than that of unmodified one. Long-duration adsorption tests showed that MCABs exhibited remarkable stability regarding their capacity and anti-fraying ability. By analyzing the structure of the material, it is demonstrated that the material is transformed from dense crosslinking polymer to organic-inorganic mineralization framework with large specific surface area and high porosity by self-

assembly mineralization. Meanwhile, with the confined crystallization of calcium ions, the carboxylic groups in the structure can be activated, making more binding sites for mercury ions.

## Supplementary Information

The online version contains supplementary material available at…


## Acknowledgments

The authors are grateful to the Analytical and Testing Center at Huazhong University of Science and Technology, Wuhan, China.

## Funding

The current work was funded by the National Natural Science Foundation of China [grant number 52106242]; Postdoctoral Research Foundation of China [grant number 2020M672350]; and the Foundation of State Key Laboratory of Coal Combustion [grant number FSKLCCA1904].


## Declarations

**Conflict of Interest** The authors declare that they have no known competing financial interests or personal relationships that could have appeared to influence the work reported in this paper.

437 **References**

438 1. A. J. Poulain and T. Barkay, Science **339**, 1280 (2013).

439 2. E. Menger-Krug, J. Niederste-Hollenberg, T. Hillenbrand, and H. Hiessl,
440 Environmental Science and Technology **46**, 11505 (2012).

441 3. B. Zhang, P. Xu, Y. Qiu, Q. Yu, J. Ma, H. Wu, G. Luo, M. Xu, and H. Yao, Chemical
442 Engineering Journal **263**, 1 (2015).

443 4. M. Xu, Y. Qiao, C. Zheng, L. Li, and J. Liu, Combustion and Flame **132**, 208 (2003).

444 5. G. Luo, H. Yao, M. Xu, R. Gupta, and Z. Xu, Proceedings of the Combustion Institute
445 **33**, 2763 (2011).

446 6. M. Xu, D. Yu, H. Yao, X. Liu, and Y. Qiao, Proceedings of the Combustion Institute
447 **33**, 1681 (2011).

448 7. Y. Dunxi, X. Minghou, Y. Hong, S. Jiancai, L. Xiaowei, Y. Yun, and C. Qian,
449 Proceedings of the Combustion Institute **31**, 1921 (2007).

450 8. Y. Zhang, D. Kogelnig, C. Morgenbesser, A. Stojanovic, F. Jirsa, I. Lichtscheidl-
451 Schultz, R. Krachler, Y. Li, and B. K. Keppler, Journal of Hazardous Materials **196**,
452 201 (2011).

453 9. F. Li, J. Zhang, W. Jiang, C. Liu, Z. Zhang, C. Zhang, and G. Zeng, Environmental
454 Geochemistry and Health 2016 39:4 **39**, 923 (2016).

455 10. J. Huang, F. Li, G. Zeng, W. Liu, X. Huang, Z. Xiao, H. Wu, Y. Gu, X. Li, X. He,
456 and Y. He, Science of The Total Environment **541**, 969 (2016).

457 11. U. Farooq, J. A. Kozinski, M. A. Khan, and M. Athar, Bioresource Technology **101**,

458 5043 (2010).
459 12. X. Gong, T. Wu, Y. Qiao, and M. Xu, Energy and Fuels **24**, 84 (2009).
460 13. J. He and J. P. Chen, Bioresource Technology **160**, 67 (2014).
461 14. I. Moreno-Garrido, Bioresource Technology **99**, 3949 (2008).
462 15. M. F. Abou Taleb, H. Albalwi, and F. I. Abou El Fadl, Journal of Inorganic and
463 Organometallic Polymers and Materials 2021 31:4 **31**, 1825 (2021).
464 16. P. Hadi, M. H. To, C. W. Hui, C. S. K. Lin, and G. McKay, Water Research **73**, 37
465 (2015).
466 17. H. Hadjar, B. Hamdi, and Z. Kessasia, Desalination **167**, 165 (2004).
467 18. R. Khosravi, A. Azizi, R. Ghaedrahmati, V. K. Gupta, and S. Agarwal, Journal of
468 Industrial and Engineering Chemistry **54**, 464 (2017).
469 19. M. Kobya, E. Demirbas, E. Senturk, and M. Ince, Bioresource Technology **96**, 1518
470 (2005).
471 20. I. Enniya, L. Rghioui, and A. Jourani, Sustainable Chemistry and Pharmacy **7**, 9
472 (2018).
473 21. R. R. Bansode, J. N. Losso, W. E. Marshall, R. M. Rao, and R. J. Portier,
474 Bioresource Technology **89**, 115 (2003).
475 22. J. Wang and C. Chen, Bioresource Technology **160**, 129 (2014).
476 23. W. S. W. Ngah and S. Fatinathan, Chemical Engineering Journal **143**, 62 (2008).
477 24. B. Liu, D. Wang, G. Yu, and X. Meng, Journal of Ocean University of China 2013
478 12:3 **12**, 500 (2013).

479 25. G. Crini and P. M. Badot, Progress in Polymer Science **33**, 399 (2008).
480 26. Y. Zhu, J. Hu, and J. Wang, Journal of Hazardous Materials **221–222**, 155 (2012).
481 27. N. Li and R. Bai, Separation and Purification Technology **42**, 237 (2005).
482 28. A. Alvarez, J. M. Saez, J. S. Davila Costa, V. L. Colin, M. S. Fuentes, S. A. Cuozzo,
483 C. S. Benimeli, M. A. Polti, and M. J. Amoroso, Chemosphere **166**, 41 (2017).
484 29. A. Talaiekhozani and S. Rezania, Journal of Water Process Engineering **19**, 312
485 (2017).
486 30. K. Vijayaraghavan and Y. S. Yun, Biotechnology Advances **26**, 266 (2008).
487 31. P. Gupta and B. Diwan, Biotechnology Reports **13**, 58 (2017).
488 32. H. Etesami, Ecotoxicology and Environmental Safety **147**, 175 (2018).
489 33. S. H. Liu, G. M. Zeng, Q. Y. Niu, Y. Liu, L. Zhou, L. H. Jiang, X. fei Tan, P. Xu, C.
490 Zhang, and M. Cheng, Bioresource Technology **224**, 25 (2017).
491 34. C. H. Kang, Y. J. Kwon, and J. S. So, Ecological Engineering **89**, 64 (2016).
492 35. Y. Feng, Y. Yu, Y. Wang, and X. Lin, Current Microbiology 2007 55:5 **55**, 402
493 (2007).
494 36. V. M. Martínez-Juárez, J. F. Cárdenas-González, M. E. Torre-Bouscoulet, and I.
495 Acosta-Rodríguez, Bioinorganic Chemistry and Applications **2012**, (2012).
496 37. H. Xiao and J. J. Zhong, Trends in Biotechnology **34**, 242 (2016).
497 38. G. Bayramoğlu, I. Tuzun, G. Celik, M. Yilmaz, and M. Y. Arica, International
498 Journal of Mineral Processing **81**, 35 (2006).
499 39. H. X. Chang, Q. Fu, Y. Huang, A. Xia, Q. Liao, X. Zhu, Y. P. Zheng, and C. H. Sun,

Bioresource Technology **219**, 668 (2016).

40. W. M. Ibrahim, Journal of Hazardous Materials **192**, 1827 (2011).

41. Y. Liu, Q. Cao, F. Luo, and J. Chen, Journal of Hazardous Materials **163**, 931 (2009).

42. V. J. P. Vilar, C. M. S. Botelho, J. M. Loureiro, and R. A. R. Boaventura, Bioresource Technology **99**, 5830 (2008).

43. N. AKHTAR, M. IQBAL, S. I. ZAFAR, and J. IQBAL, Journal of Environmental Sciences **20**, 231 (2008).

44. P. X. Sheng, K. H. Wee, Y. P. Ting, and J. P. Chen, Chemical Engineering Journal **136**, 156 (2008).

45. M. Y. Arica, Ç. Arpa, B. Kaya, S. Bektaş, A. Denizli, and Ö. Genç, Bioresource Technology **89**, 145 (2003).

46. G. T. Grant, E. R. Morris, D. A. Rees, P. J. C. Smith, and D. Thom, FEBS Letters **32**, 195 (1973).

47. D. Bulgariu and L. Bulgariu, Bioresource Technology **103**, 489 (2012).

48. E. Bağda, M. Tuzen, and A. Sarı, Journal of Environmental Radioactivity **175–176**, 7 (2017).

49. A. R. Khataee, F. Vafaei, and M. Jannatkhah, International Biodeterioration & Biodegradation **83**, 33 (2013).

50. W. Plazinski, Adsorption 2013 19:2 **19**, 659 (2013).

51. Y. H. Huang, P. K. Peddi, C. Tang, H. Zeng, and X. Teng, Separation and Purification Technology **118**, 690 (2013).

52. M. Hadavifar, N. Bahramifar, H. Younesi, and Q. Li, Chemical Engineering Journal **237**, 217 (2014).

53. M. Zuber, F. Zia, K. M. Zia, S. Tabasum, M. Salman, and N. Sultan, International Journal of Biological Macromolecules **80**, 366 (2015).

54. X. Li, Q. Shen, Y. Su, F. Tian, Y. Zhao, and D. Wang, Crystal Growth and Design **9**, 3470 (2009).

55. P. Diaz-Rodriguez, P. Garcia-Triñanes, M. M. Echezarreta López, A. Santoveña, and M. Landin, Carbohydrate Polymers **195**, 235 (2018).

56. Y. Ma, J. Zhang, S. Guo, J. Shi, W. Du, Z. Wang, L. Ye, and W. Gu, Materials Science and Engineering: C **68**, 551 (2016).

57. J. Zhao, X. He, L. Wang, J. Tian, C. Wan, and C. Jiang, International Journal of Hydrogen Energy **32**, 380 (2007).

58. V. J. P. Vilar, C. M. S. Botelho, and R. A. R. Boaventura, Process Biochemistry **40**, 3267 (2005).

59. S. C. Ponce, C. Prado, E. Pagano, F. E. Prado, and M. Rosa, Ecological Engineering **74**, 33 (2015).

60. E. N. Bakatula, E. M. Cukrowska, I. M. Weiersbye, L. Mihaly-Cozmuta, A. Peter, and H. Tutu, Journal of Geochemical Exploration **144**, 492 (2014).

61. D. Kratochvil and B. Volesky, Trends in Biotechnology **16**, 291 (1998).

62. H. Qiu, L. Lv, B. Pan, Q. Zhang, W. Zhang, and Q. Zhang, Journal of Zhejiang University-SCIENCE A 2009 10:5 **10**, 716 (2009).

542 63. V. J. P. Vilar, C. M. S. Botelho, and R. A. R. Boaventura, Journal of Hazardous
543 Materials **143**, 396 (2007).
544 64. X. Li, Q. Shen, Y. Su, F. Tian, Y. Zhao, and D. Wang, Crystal Growth and Design **9**,
545 3470 (2009).
546

# Supplementary Files

This is a list of supplementary files associated with this preprint. Click to download.

- SupplementaryMaterial.docx